The use of pulse-compression thermography for detecting defects in paintings

S.Laureti[1], S.Sfarra[2], H.Malekmohammadi[1], Pietro Burrascano[1], David. A. Hutchins[3], Luca Senni[1], G. Silipigni[1], X.P.V. Maldague[4], and Marco Ricci[5]

[1]Department of Engineering, Polo Scientifico Didattico di Terni, University of Perugia,
Strada di Pentima 4, 05100 Terni, Italy
{stefano.laureti,hamed.malekmohammadi,pietro.burrascano,luca.senni}@unipg.it, giuseppe_silipigni@hotmail.com
[2]Department of Industrial and Information Engineering and Economics, University of L'Aquila, Piazzale E. Pontieri 1, 67100
Loc. Monteluco di Roio – L'Aquila (AQ), Italy
stefano.sfarra@univaq.it
[3]School of Engineering, University of Warwick
Library Road, Coventry CV4 7AL, United Kingdom
D.A.hutchins@warwick.ac.uk
[4]Department of Electrical and Computer Engineering, Laval University, 1065,
av. de la Médecine, G1V 0A6 Québec city, Canada QC
e-mail: Xavier.Maldague@gel.ulaval.ca
[5]Department of Informatics, Modeling, Electronics and Systems Engineering, University of Calabria,
Via Pietro Bucci, 87036 Arcavacata, Rende CS, Italy
e-mail: m.ricci@dimes.unical.it

***Abstract*—**The interest towards the conservation of cultural goods grows year by year. Their periodic inspection is essential for their conservation over the time. Thermographic nondestructive inspection is one technique useful for paintings, but it is essential to be able to detect buried defects while minimising the level of thermal stimulus. This paper describes a pulse-compression infrared thermography technique whereby defect detection is optimised while minimising the rise in temperature. To accomplish this task, LED lamps driven by a coded waveform based on a linear frequency modulated chirp signal have been used on paintings on both a wooden panel and a canvas layer. These specimens contained artificially fabricated defects. Although the physical conditions of each painting were different, the experimental results show that the proposed signal processing procedure is able to detect defects using a low temperature contrast.

Keywords*—Thermography, Coded Excitation, Pulse-compression, Cultural heritage.*

I. INTRODUCTION

Active Thermography (AT) is a Non-Destructive Evaluation (NDE) technique widely used in different fields of research and industrials applications, as in material characterization [1], food inspection [2] and in cultural heritage diagnostic [3]. AT always relies on exciting the sample with a heating stimulus to achieve the required thermal contrast, though many different measurement schemes and post-processing algorithms can be employed [4]. For cultural heritage objects, AT is commonly implemented using Pulsed Thermography (PT), where the sample *e.g.* a bookbinding [5], bronze statue [6] or painting [7] is excited by an impulse from a flash lamp. Additional thermal stimuli that have been reported include hot air [8], cold air [9], quartz lamps linear systems [10], heating plates [11], halogen lamps [12] and laser heating [13]. Information about defects and other structural changes are retrieved by analysing both the heating and cooling response as a function of time and location.

Although PT is relatively simple to use and provides an easy and meaningful data processing, care should be taken when applying pulsed stimulus to cultural objects such as paintings, as abrupt variations of the sample temperature, potentially resulting in dangerous thermal shocks, may occur, although these can be anticipated using numerical simulations centred on heat transfer phenomena [14,15]. In particular, colour changes (known

as thermochromism) may result – a particular pigment may react to long (or repetitive) exposures to high temperatures so as to degrade the perceived colour. In other instances, an exposed area may drift to another shade of colour. Certain colours formed by pigments are more susceptible to this drift [16]. For example, in vivianite ($Fe_3(PO_4)_2 \cdot 8H_2O$, blue), heat-related damage can be observed at temperatures as low as 70 °C, causing colour changes in both pure vivianite [17] and oil paint layers containing it [18]. Thus, minimising the temperature variation is of primary importance.
The use of low-power excitation is therefore desirable in such cases, but this leads to a significant reduction of the Signal to Noise Ratio (SNR) that could affect the effectiveness of the PT analysis.
Fortunately, techniques have been developed capable of improving the SNR of AT measurements in case of low-power sources. One approach is Lock-in Thermography (LT), where the heating stimulus is modulated at a specific frequency [19]. The acquired thermograms are then processed in the frequency domain, thus obtaining phase and magnitude images of the investigated item at that frequency [20]. LT is widely adopted as it provides a significant gain of SNR. However, the depth of penetration is set by the modulation frequency and the output info is few compared with that of PT, which excites a greater measurement bandwidth [21]. Therefore, efforts have been made to combine the advantages of both schemes, leading for example to Pulse Phase Thermography [22], and the more complex Multi-Frequency Lock-in Thermography [23].
Another possible choice to accomplish this aim is the Pulse-Compression Thermography (PuCT), first introduced by Tabatabaei and Mandelis [24], and recently developed by other groups [25,26]. In fact, the Pulse Compression (PuC) algorithm outputs an accurate impulse response estimate that is very similar to that obtainable from PT, even when low-power sources are used. The employed modulated heating stimulus is here in the form of a coded excitation where the bandwidth B and the duration T of the signal are uncorrelated. Hence, the frequency content of the coded signal can be tailored to suit the investigation of a given sample, while T can be increased almost arbitrarily to achieve the desired SNR [27–30]. These properties can be usefully applied to inspect cultural heritage objects, using low-power heating sources to keep surface temperatures relatively low. Moreover, the use of coded excitations and PuC allows both frequency and time domain analyses to be performed. A frequency domain analysis can be carried out directly on the raw acquired data; the time domain analysis can be executed after the application of the PuC algorithm. It is worth to note that the use of pseudo-random modulated heating stimulus has been introduced so far in infrared thermography [31], and recently applied even in AT for cultural heritage diagnostic by Candoré *et al* [32]. However, in these works the thermal impulse response of the Sample Under Test (SUT) is estimated by using an Auto Regressive Moving Average algorithm (ARMA) to model the process. In PuCT instead, the thermal impulse response of the SUT is estimated by applying a deterministic procedure based on the application of the so called matched filter. In addition, in [32] the thermal source consists of halogen lamps driven by a pseudo-random code while in the present paper the heating stimulus is realized with LEDs driven by a chirp signal.

The aim of this paper is to propose the employment of the PuCT scheme for the NDE of paintings. PuCT has been performed on two different artificially-realised specimens, representing two painting types: one being a painted wooden panel [33,34] the other a painting on canvas [35,36]. They each contain artificially fabricated defects as briefly described in the next section. It should be noted that each of these samples aims to mimic the painting technique of a specific artistic period. In particular, the panel painting was constructed following the Cennino Cennini's rules [37], while the painting on canvas is close to the contemporary art, where a different the type of paint was used [38]. Therefore, the artistic period to which they refer is completely different. For the current setup, the heating source consisted of eight LED chips which provided an overall power of 110W, low enough to avoid overheating of the sample. The coded waveform chosen for this work is a linear frequency modulated chirp signal, a sinusoidal signal whose frequency varies linearly as time elapses. It is worth noting that the instantaneous chirp amplitude varies smoothly with time. Thus, the combined use of PuC and an *ad hoc* designed linear chirp was able to damp any thermal shock for the investigated Sample Under Test (SUT) with respect to PT, while maintaining the sample temperature increment relatively low.

II. DESCRIPTION OF THE SAMPLES

In this section, the main information regarding the fabrication of the paintings are reported.

II.A Painting on canvas

In this case, a linen canvas was used as support. After a treatment with glue, the canvas was fixed on a wooden frame. A crayon drawing was realized on the canvas (Fig. 1(a)); it was covered by several layers. Two fabricated defects were inserted at different depths. These defects are made by Mylar, see Fig. 1(b). In particular, defect A (4.5 x 1 cm) consists of two superimposed Mylar layers, defect B (4 x 1 cm) is formed by one layer. The defects were fixed between the size and the ground layers, see Fig. 1(b) and (d). Then, the canvas was sewed up (see the arrows in Fig. 1(c)), and other repairs were realized using a crochet-hook. The upper layers are shown in Fig. 1(d), while the final sample is reported in Fig. 1(e). In this case, an acrylic paint was used.

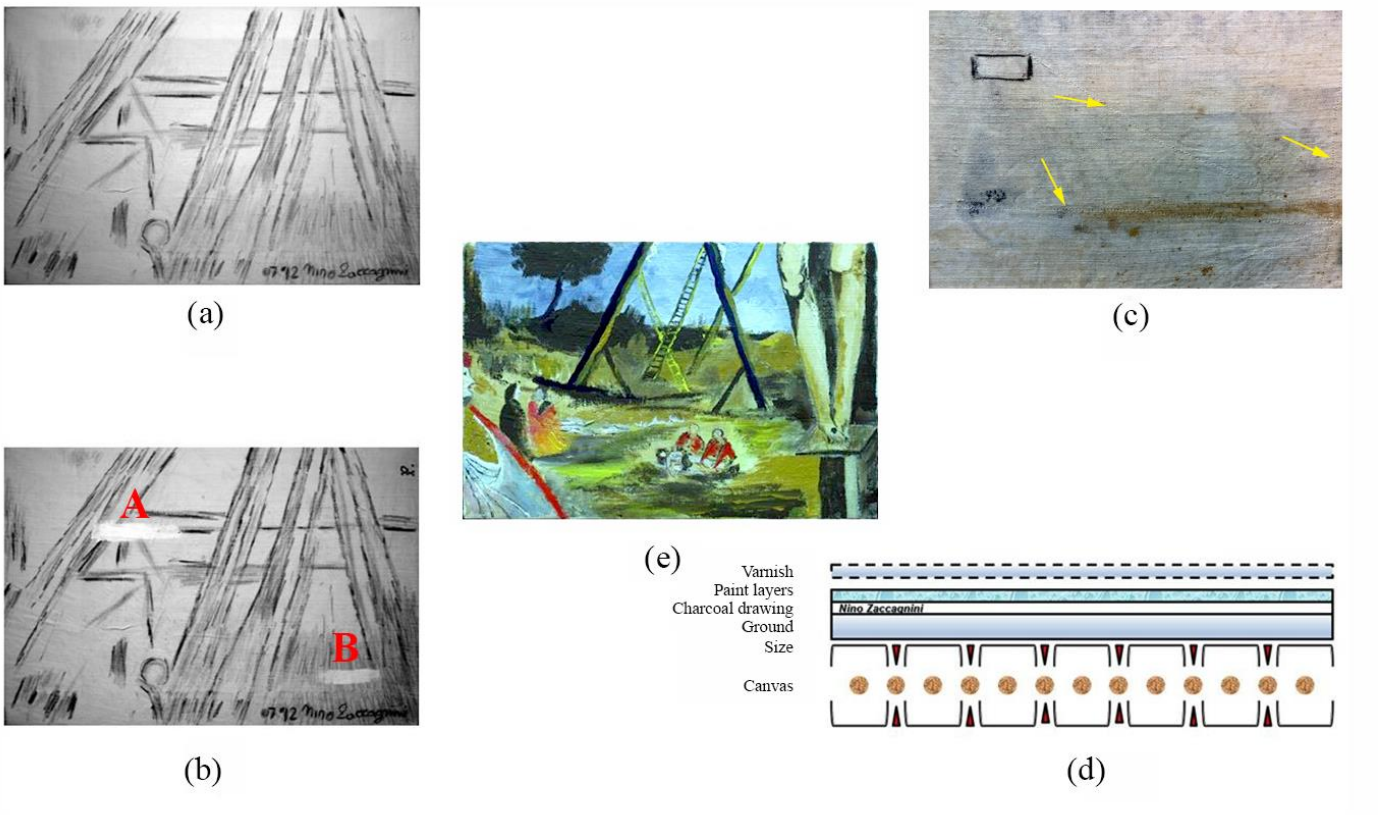

Fig. 1 Painting on canvas: (a) the preparatory drawing, (b) defects A, B, (c) back view with embroideries, (d) the layers constituting the sample, and (e) front view of the final sample.

II. B wooden panel painting

The panel painting, based on a poplar wood substrate with dimensions (20 x 25 x 2 cm), is shown in Fig. 2(a) along with the positions of the defects (labelled C-D). Poplar was frequently used for the fabrication of panel paintings in the Italian schools [37]. Splitting areas were simulated by inserting a Mylar sheet (defect C) and a thin sponge covered with Mylar (defect D) at different depths beneath the paint layer. The gilding layer was not applied in this case, while oil colours where used to finalize the sample. Other satellite defects were also possibly present due to the nature of poplar wood, which is normally soft, weak, fine-grained, diffuse-porous, with small pores in term of size [39].

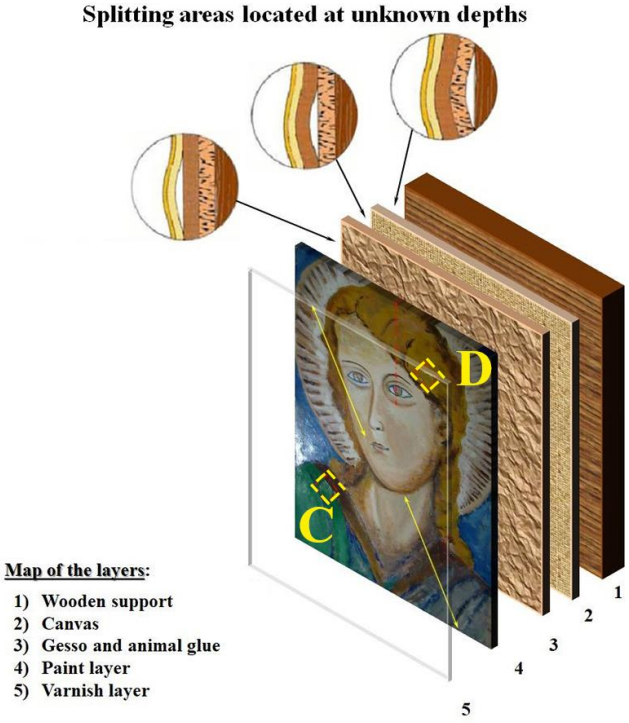

Fig. 2 Panel painting: front side and position of the defects and layers.

III. THEORETICAL BACKGROUND

Heat transfer is a very complex phenomenon for which many references can be found in literature. The reader is referred to [40–42] for a detailed mathematical description of the heat transfer within a body when AT is performed, particularly for the case of PuCT [25,26].
The following subsections are aimed at showing the basic mathematical theory at the heart of PuCT, its pros and cons with respect to standard pulsed excitation, and how to correctly apply this technique for NDE. Moreover, the main features of the employed linear chirp signal are also shown.

III.A Pulse-Compression basic theory

PuC is a measurement technique employed to estimate the impulse response $h(t)$ of Linear Time Invariant (LTI) systems in poor SNR conditions. In standard PT, flash lamps are usually exploited to heat the sample within a time significantly shorter than the typical cooling time of the sample itself. Thus, the heating stimulus exciting the LTI system can be modelled as a Dirac's Delta function $\delta(t)$ so that the corresponding impulse response $h(j_x, j_y, t)$ is directly retrieved as the pixel temperature/emissivity time trend (see Fig.3(a)). Useful information about the sample are obtained by analysing both the heating and the cooling of the $\{h(j_x, j_y, t)\}$ within a chosen range of interest T_h. PuCT requires further processing steps to be performed, as it relies on the existence of two signals $\{s(t), \Psi(t)\}$ such that their convolution $\tilde{\delta}(t)$ approximates the Dirac's Delta Function $\delta(t)$:

$$s(t) * \Psi(t) = \tilde{\delta}(t) \approx \delta(t) \quad (1)$$

where * denotes a convolution, $s(t)$ is the coded excitation of duration T and bandwidth B, and $\Psi(t)$ is the so-called matched filter. If Eq.(1) holds, an estimate $\tilde{h}(j_x, j_y, t)$ of the $h(j_x, j_y, t)$ is obtained by exciting the LTI system with $s(t)$ and then by convolving the acquired system output $y(j_x, j_y, t)$ with $\Psi(t)$, see Fig.3(b). This is

demonstrated in Eq. (2) for a single pixel of the acquired image, where also the presence of an Additive-White-Gaussian-Noise (AWGN) as the $e(t)$ term, uncorrelated to $\Psi(t)$), is considered.

$$\tilde{h}(t) = y(t) * \Psi(t) = h(t) * \underbrace{s(t) * \Psi(t)}_{=\tilde{\delta}(t)} + e(t) * \Psi(t) = h(t) * \tilde{\delta}(t) + \tilde{e}(t) \approx h(t) + \tilde{e}(t) \quad (2)$$

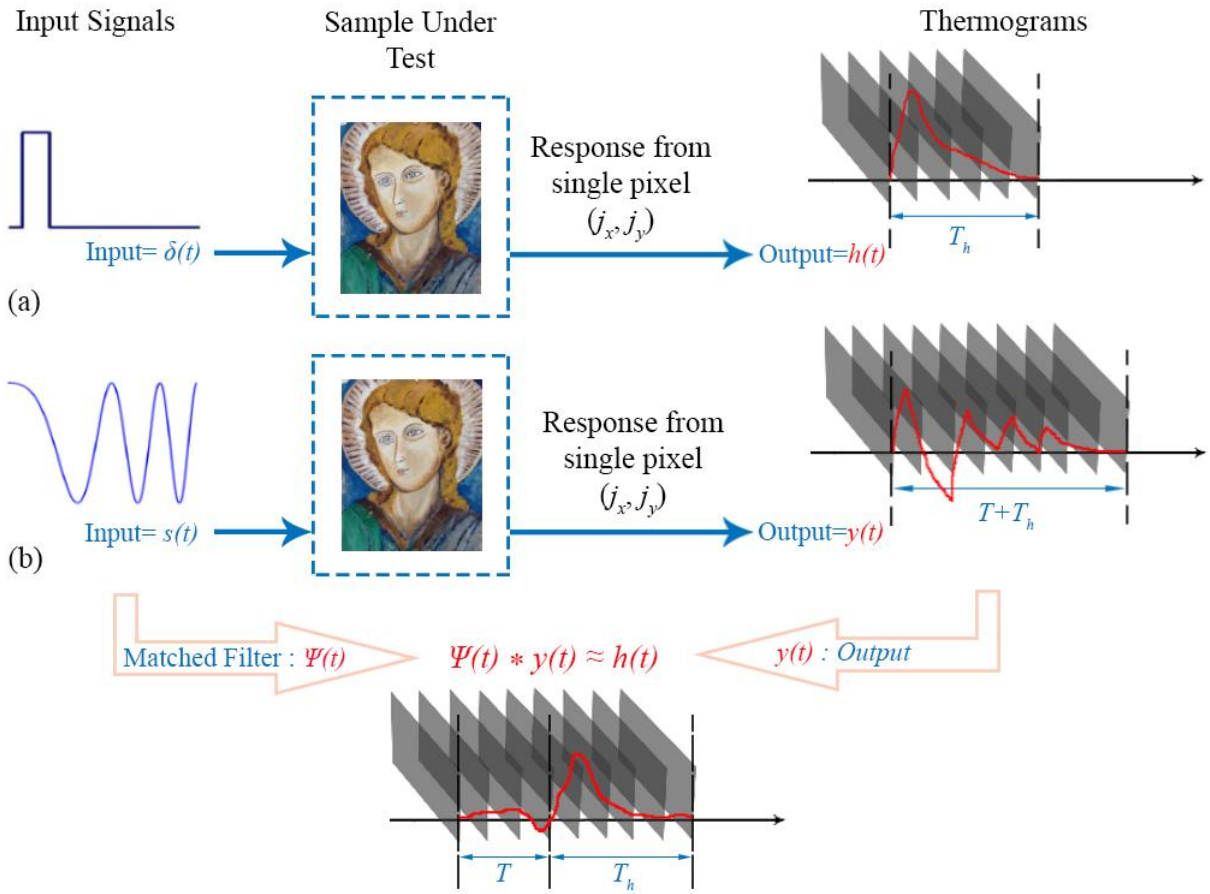

Fig. 3 Comparison between (a) Pulsed Thermography (PT) and (b) Pulse-Compression Thermography (PuCT). In PT the excitation is considered instantaneous and the sample impulse thermal response is measured for a time T_h, which is the impulse response time duration, *i.e.* the time necessary for the diffusion of the heat. In PuCT, the sample is excited with a coded excitation of duration T and thermograms are collected for an overall time duration of $T+T_h$. After the application of the PuC algorithm, an estimated impulse thermal response of duration T_h is retrieved.

The use of PuC instead of pulsed excitation results in an estimate $\tilde{h}(t)$ of the $h(t)$ having an increased SNR. The SNR gain is proportional to the $T \cdot B$ product, *i.e.* it can be enhanced almost arbitrarily by increasing either the time duration or the bandwidth of the coded waveform. Under the hypothesis of AWGN noise, the use of a matched filter defined as $\Psi(t) = s(-t)$ maximizes the SNR for a given setup [43]. Drawbacks of the use of PuC arise from the practically-limited T and B values that lead to an approximated reconstruction of the Dirac's Delta $\tilde{\delta}(t)$ and hence of the impulse responses. Only an approximation $\tilde{h}(j_x, j_y, t)$ can be retrieved after PuC, the quality of this approximation, depending on the levels of sidelobes associated with $\tilde{\delta}(t)$. Therefore, it is important to reduce the magnitude of the sidelobes, as they can reduce the defect detection capability. Many studies can be found showing different approaches for optimizing the design of both the coded waveform and

the matched filter, either for decreasing the $\tilde{\delta}(t)$ sidelobes magnitude or for maximizing the SNR gain. Although an exhaustive investigation lies beyond the scope of the present work, it has been observed that replacing the standard matched filter with a Wiener filter helps on minimizing $\tilde{\delta}(t)$ sidelobe magnitudes [43–45] . Finally, the $\tilde{\delta}(t)$'s reconstruction quality strictly depends on the correct implementation of the convolution procedure. The reader is referred to [25,46–51] for further details.

III.B. Linear Chirp Signal and Optimized Wiener Filter

A linear chirp signal is a frequency modulated signal whose instantaneous frequency varies linearly within a chosen range. A general mathematical definition of a chirp is given here:

$$s(t) = \cos\left(\phi(t)\right) \tag{3}$$

with $\phi(t)$ the instantaneous signal phase. The design of a chirp strictly depends from the definition of the instantaneous frequency $f_{ist}(t)$:

$$f_{ist}(t) = \frac{1}{2\pi}\frac{d\phi(t)}{dt} \tag{4}$$

For a linear chirp signal, the phase is a quadratic function $\phi(t) = f_0 t + \frac{B}{2T}t^2$, leading to $f_{ist}(t)$ that is a linear function of time:

$$f_{ist}(t) = f_0 + \frac{B}{T}t \tag{5}$$

where B is the bandwidth $B = f_1 - f_0$, that is the difference between the initial and the final value of the instantaneous chirp frequency. Note that if $f_1 > f_0$, $B > 0$, $f_{ist}(t)$ increases as time elapses and the chirp is called "up" linear chirp; otherwise if $f_1 < f_0$, $f_{ist}(t)$ decrease as time elapses and the chirp is a "down" linear chirp. Although an "up" linear chirp could be employed as well, hereinafter a "down" chirp signal is considered, spanning the frequency range within $f_1 = 0$ Hz and $f_0 = 1$ Hz for an overall duration of $T = 52$ s, as depicted in Fig.4(a). Please note that the selected frequency range has been chosen so as to guarantee high thermal diffusion lengths, thus allowing a high penetration within the inspected sample; in addition the chosen $T \cdot B$ is high enough to provide a sufficient SNR value [28,49]. Finally, the extended duration of the coded signal, together with its smooth instantaneous amplitude transition helps in avoid any thermal shock over the SUT, see Fig. 4(a).

As mentioned above, Wiener Filtering suppresses the magnitude of $\tilde{\delta}(t)$ sidelobes by up to 30dB with respect to what achievable by employing a matched filter $\Psi(t) = s(-t)$ without any further processing [26]. Applying Wiener filter simply consists of substituting $\Psi(t)$ with a new matched filter $\Psi_W(t)$, defined as for Eq.(6):

$$\Psi_W(t) = IFFT\left(\frac{\Psi(f)}{|\Psi(f)|^2 + a + b\cdot|f|}\right) = IFFT\left(\frac{s^*(f)}{|s(f)|^2 + a + b\cdot|f|}\right) \tag{6}$$

where IFFT stands for Inverse Fast Fourier Transform operator, a and b are two regularization parameters, the former regulating the filter effect over the entire bandwidth, the latter penalizing the high frequencies. Eq. (6) shows that $\Psi_W(t)$ has the same phase profile of the $\Psi(t)$ but with modified spectrum amplitude. Fig. 4(b)

depicts both the standard $\Psi(t)$ and the optimized $\Psi_W(t)$, whilst a comparison between the obtained $\tilde{\delta}(t)$ with the said matched filters is shown in Fig. 4(c). Fig. 4(c) shows that the use of Wiener filter $\Psi_W(t)$ leaves the main lobe amplitude almost unaltered with respect to use the standard $\Psi(t)$, while providing a significant sidelobe reduction. Therefore, the resulting $\tilde{\delta}(t)$ quality is improved, leading to a better $\tilde{h}(t)$ estimate.

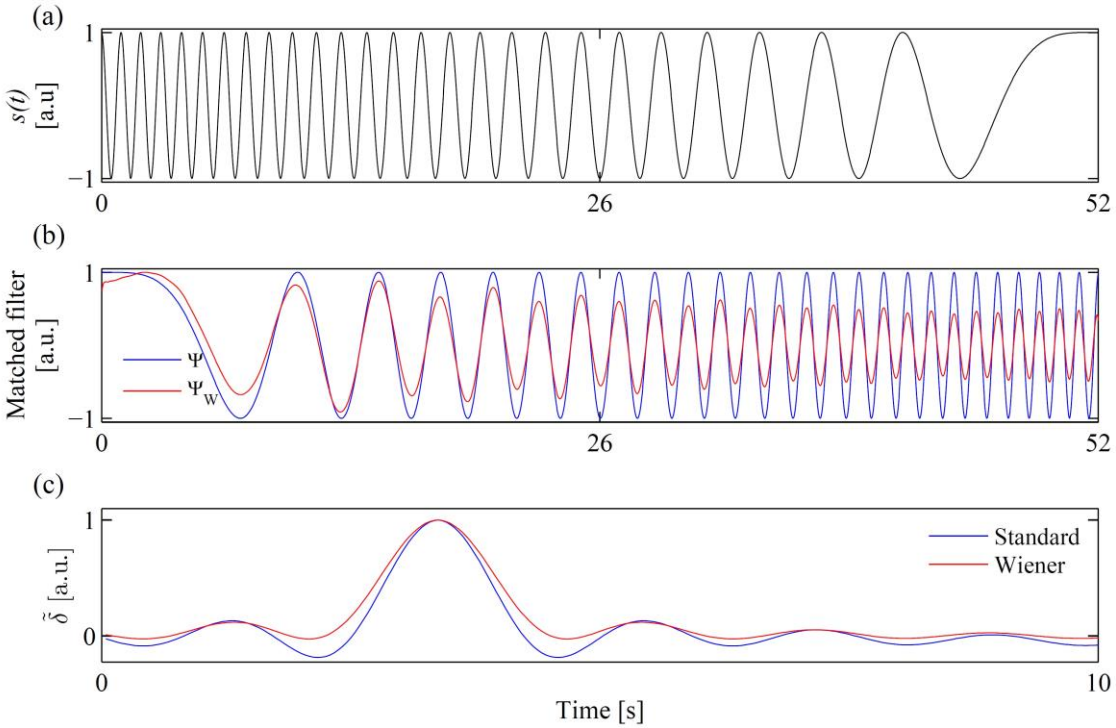

Fig. 4(a) Employed chirp signal time handling; (b) comparison between standard matched filter $\Psi(t)$ (blue) and proposes Wiener filter $\Psi_W(t)$ (red) time handling; (c) comparison between $\tilde{\delta}(t)$ obtained by using either $\Psi(t)$ (blue) or $\Psi_W(t)$ (red).

IV. The Use of Pulse Compression in Active Thermography

As already stressed, the quality of the estimated $\tilde{h}(t)$ of the real impulse response $h(t)$ obtained by performing PuC depends on the correct choice of (i) both the coded signal parameters and the related matched filter, and (ii) the correct implementation of the convolution procedure. Point (i) has been already discussed in the previous section. Regarding point (ii), issues will arise from the difficulty in realizing a bipolar heating source. Therefore, an offset must be applied over the chirp signal $s(t)$ instantaneous amplitude, so as to drive successfully the employed heating source. It thus follows that the real employed excitation signal $s_{TR}(t) = s(t) + s_{SQ}(t)$ is the superposition of a chirp signal $s(t)$ and a square pulse $s_{SQ}(t) = C\{\vartheta(t) - \vartheta(t-T)\}$ where $\vartheta(t)$ is the Heaviside step function. Thus, the true acquired output signal (Eq. (7)) will be:

$$y_{TR}(t) = h(t) * s(t) + h(t) * s_{SQ}(t) + e(t) = y(t) + y_{SQ}(t) + e(t) \tag{7}$$

Consequently, the contribution of $y_{SQ}(t)$ from $y(t)$ must be removed before finalizing the PuC algorithm via convolution with the matched filter. For clarity, this requirement can be realized by comparing Eq. (7) with Eq. (2). Recently, Silipigni *et al.* [26] proposed a procedure for proper implementing PuC in AT based on extending the $s_{SQ}(t)$ contribution for some time after T. It has been shown that this helps to design an optimized non-linear fitting algorithm, capable of correctly removing the contribution $y_{SQ}(t)$ from $y(t)$.

In summary, the PuCT procedure should use the following steps:

1) Excite the sample with a chirped heating stimulus of time duration T and with an additional $s_{SQ}(t)$ contribution for $T_{SQ} = T + T_h > T$. Here $T_{SQ} = 82s$, $T = 52s$ and $T_h = 30s$. Thus, the sample is kept heated for 30 seconds after the end of the coded stimulus.
2) Acquire thermograms for an overall time interval T_{SQ}.
3) Apply to the $y_{SQ}(t)$ the removal procedure for each pixel of the acquired thermogram sequence, thus obtaining $y(t)$.
4) Perform a pixel-by-pixel convolution of each $y(t)$ with the optimized $\Psi_W(t)$, *i.e.* retrieving the $\tilde{h}(j_x, j_y, t)$.

The true output signals are reported in Fig.5 where the role of the step-heating is highlighted as well.

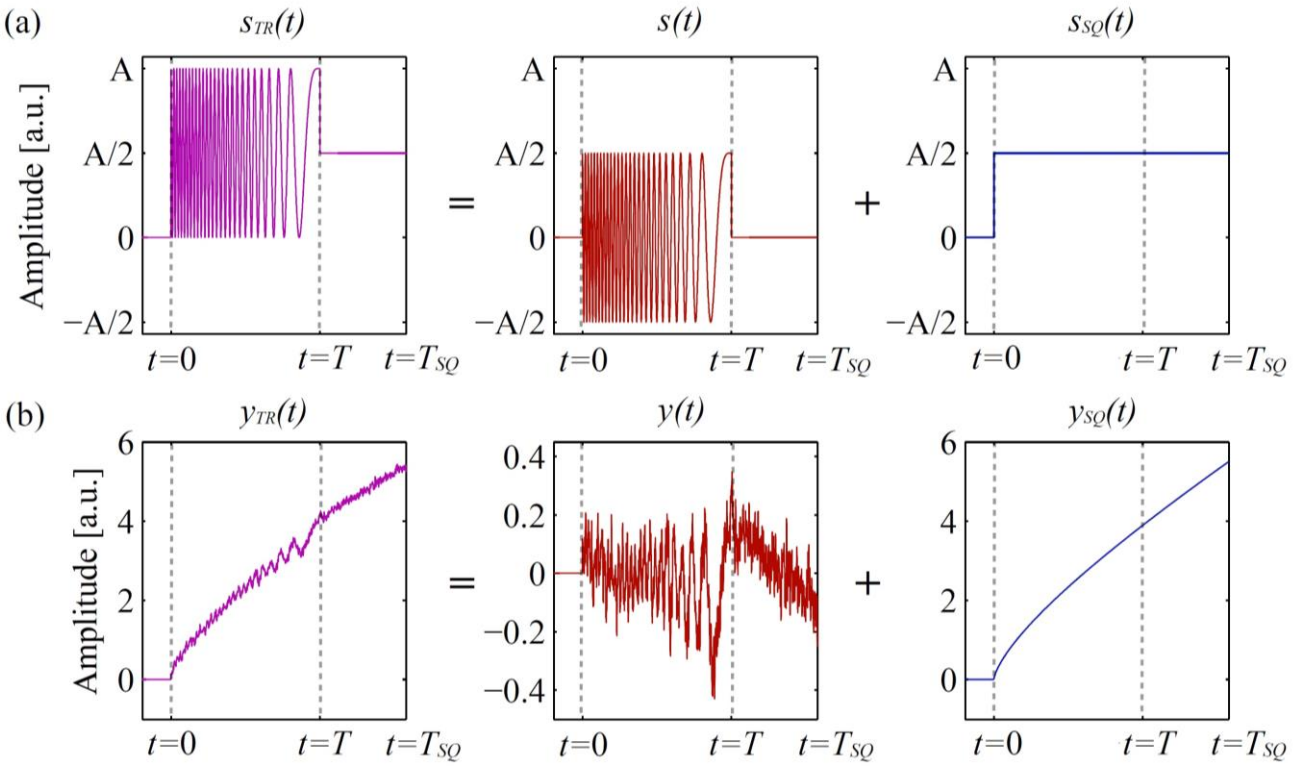

Fig. 5 (a) True excitation $s_{TR}(t)$and (b) true output $y_{TR}(t)$ signals. *y(t)* is retrieved after performing a non-linear fitting procedure to remove completely the $y_{SQ}(t)$ contribution;

V. EXPERIMENTAL SETUP

A sketch of the experimental setup used is depicted in Fig. 6.

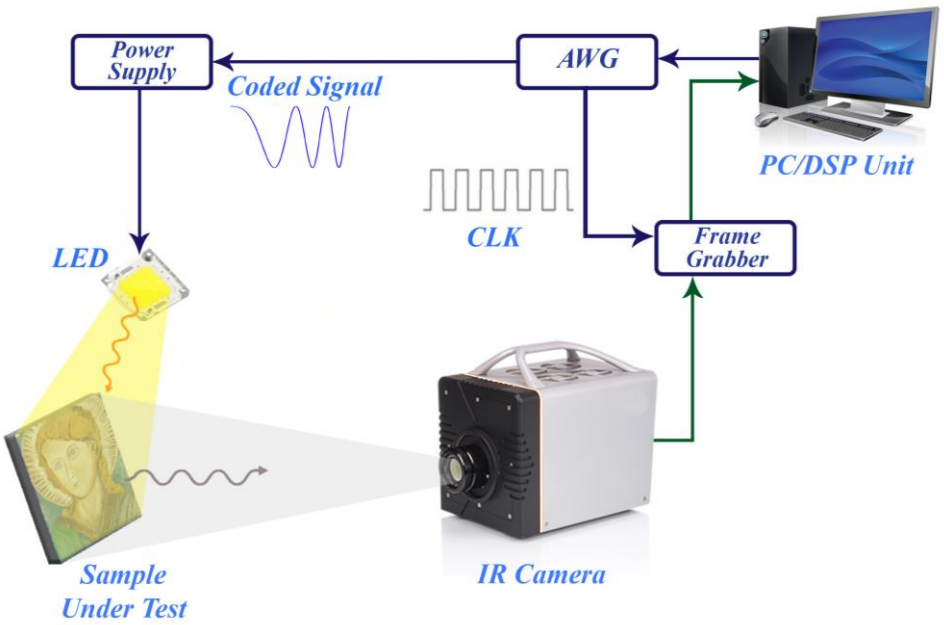

Fig. 6 The experimental setup. The Arbitrary Waveform Generator (AWG) and Frame Grabber were connected to a PC. The AWG board provided both the wanted linear chirp excitation and a reference clock signal (CLK) for triggering the IR camera acquisition. The coded signal was input into a TDK Lambda GEN 750W power supply that fed eight LED chips placed at about 30 cm from the SUT.

A National Instrument PCI-6711 Arbitrary Waveform Generator (AWG) board and a National Instrument 1433 Camera Link Frame Grabber were connected to a PC, and an ad hoc developed virtual instrument in LabVIEW^{TM} managed the signal generation/acquisition. The AWG board provided both the wanted linear chirp excitation and a reference clock signal (CLK) for triggering the IR camera acquisition, which was a Xenics Onca-MWIR-InSb IR camera. The coded signal was input into a TDK Lambda GEN 750W power supply that fed eight LED chips placed at about 30 cm from the SUT. The LED chips are capable to provide a maximum overall power of 400W but as aforementioned in the reported experiments the total employed power was reduced to 110W to avoid the overheating of the sample. In addition, the native Xenics software (Xeneth^{TM}) was used for estimating the temperature increment at the sample when excited by the chosen chirp-modulated heating stimulus. Finally, the thermograms were acquired at 40 FPS.

VI. Results

As already pointed out, it is important to keep the painting temperature increase as low as possible during the inspection. Preliminary results show that a temperature increment of ~1 °C occurred with the employed setup at the sample surface. This is illustrated in Fig. 7, where the temperature profile averaged over a line of pixels (1-2) crossing the panel painting surface is plotted as the time elapsed.

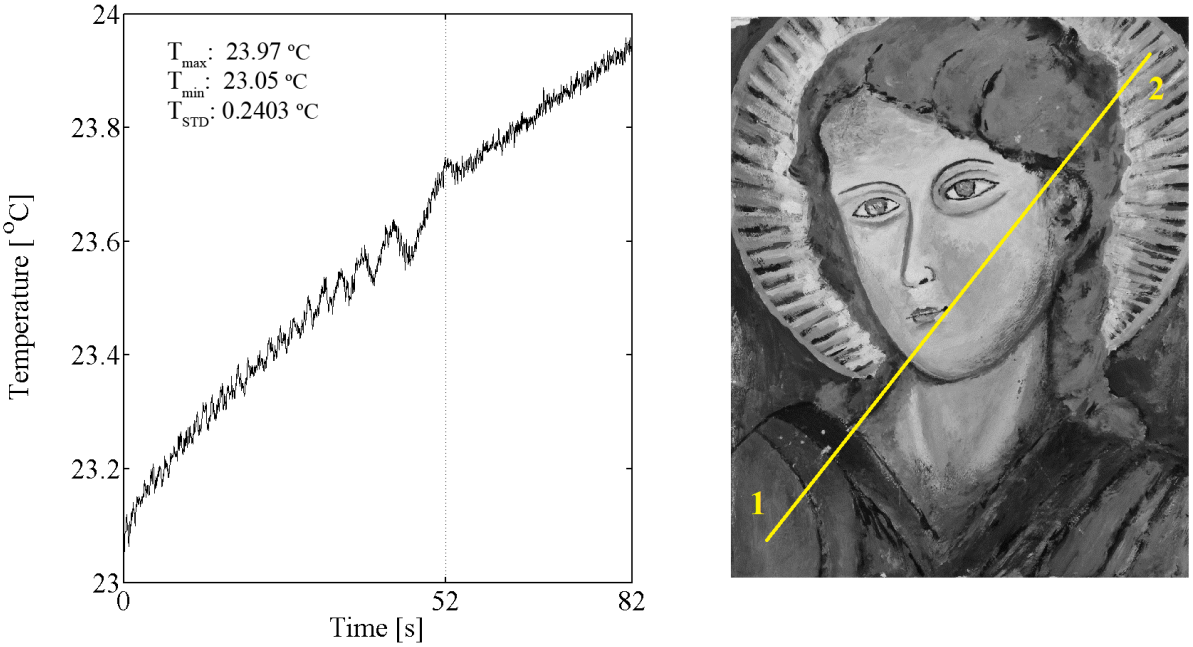

Fig. 7. Averaged temperature time handling of a line of pixels (1-2) crossing the panel painting surface while subject to the employed heating stimulus. Maximum (T_{max}), minimum (T_{min}) and standard deviation (T_{STD}) values are reported inside the plot.

Figs. 8 and 9 show the effect of the overall PuC procedure on defect detection and resolution by reporting a graphical comparison between thermograms collected during both the application of the chirp excitation (Figs. 8(a) and 9(a)) and after PuC (Figs. 8(b) and 9(b)). An improvement in the SNR of the image is clearly visible after PuC with respect to the acquired raw data. Also, areas containing defects appeared as bright pixels areas on the sliced thermogram sequences after PuC (Figs. 8(b) and 9(b)).

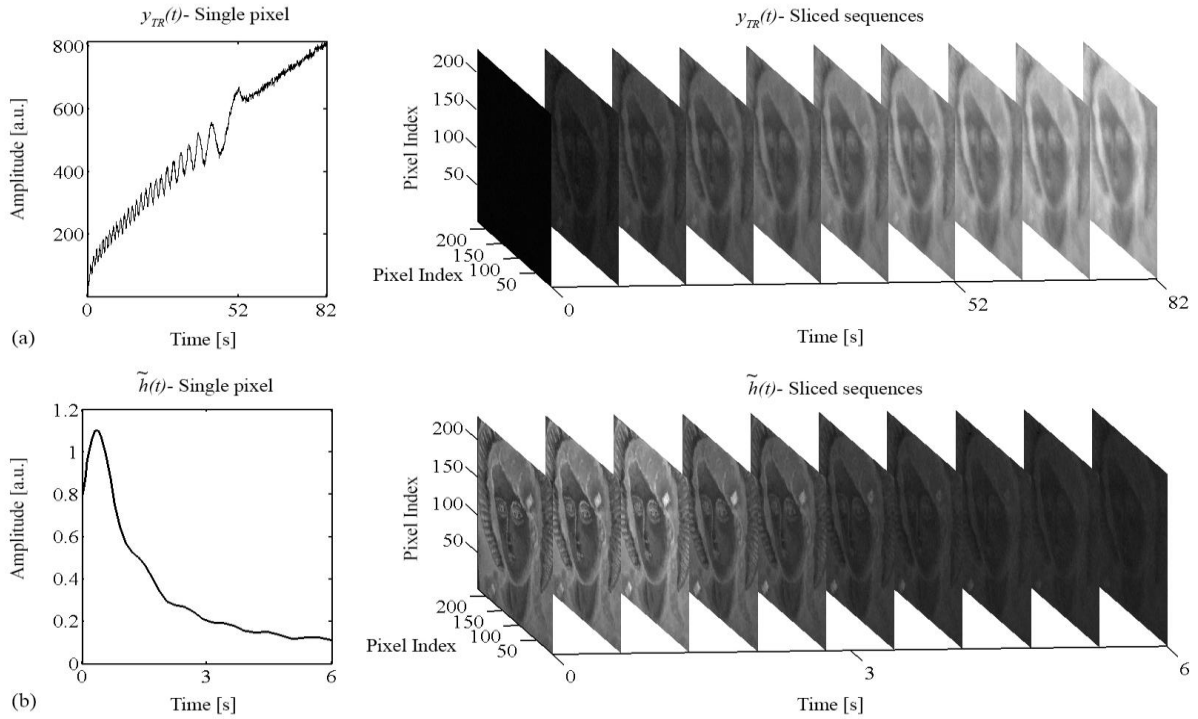

Fig. 8 (a) Comparison between thermograms collected at different times during the application of the chirp excitation; (b) thermograms retrieved after pulse compression, panel painting.

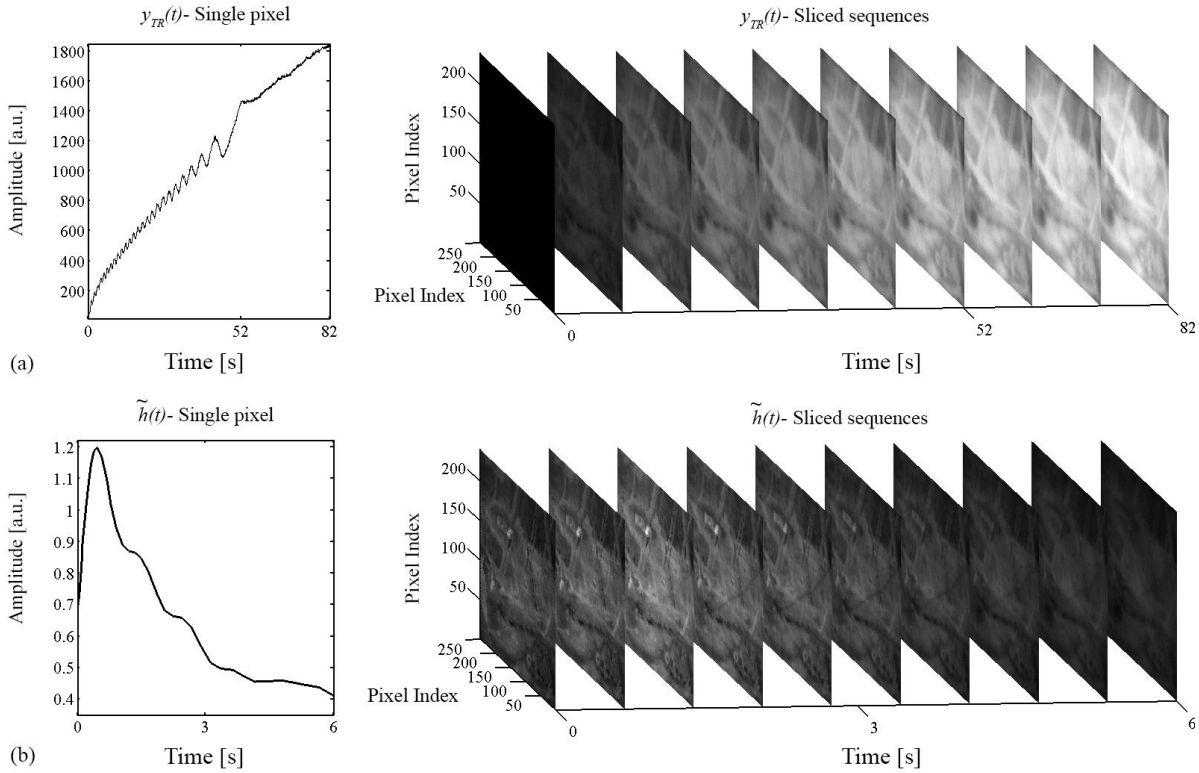

Fig. 9 (a) Comparison between thermograms collected at different times during the application of the chirp excitation; (b) thermograms retrieved after pulse compression, canvas painting.

Fig.10 depicts two frames selected for both the canvas (Fig. 10(a)) and the panel sample (Fig. 10(b)) in which the defected areas detected are highlighted by yellow markers. These frames have been selected after a qualitative analysis of the recovered thermograms after PuC, *i.e.* by selecting the frames at which the defected areas appear to be clearly visible. The subsurface embroideries realized in the canvas layer of the painting on canvas are also detectable. They are indicated by arrows in Fig. 10(a).

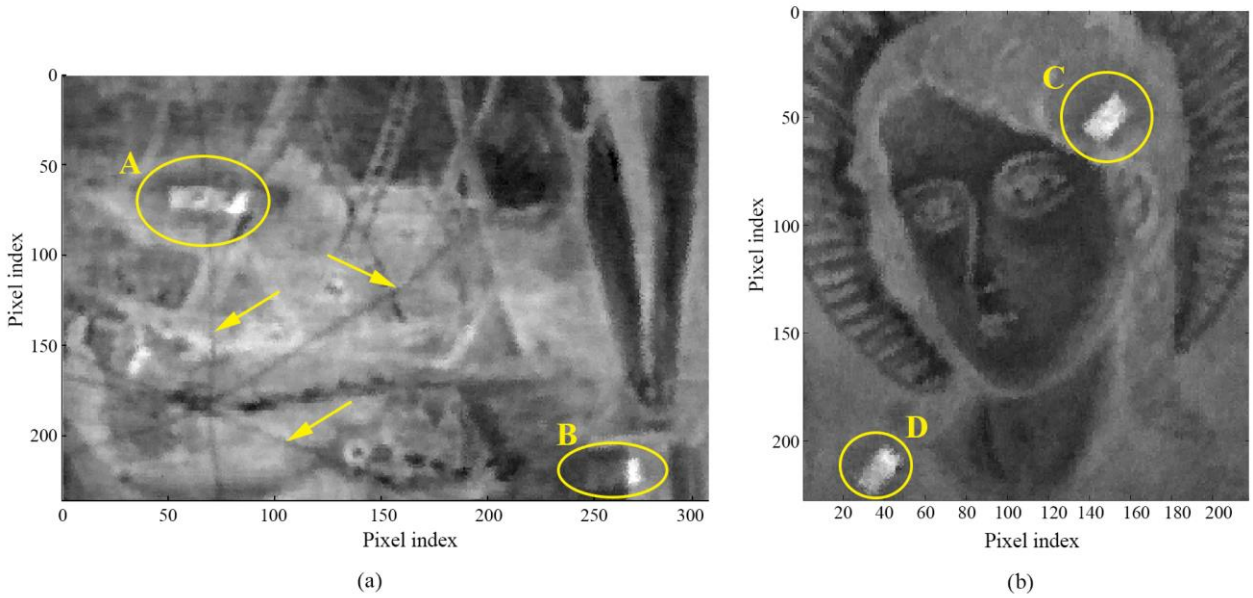

Fig. 10 Selected best frames after PuC for the (a) canvas and (b) panel painting. Yellow markers show defect A-B-C-D and embroideries.

It is important to stress out that the use of a coded heating stimulus provides the possibility to perform a simultaneous frequency and time analysis directly on the raw data (see Fig. 8(a)). In order to have a comparison of the results obtained with PuCT and another AT technique, a LT experiment was conducted. Since the selection of the optimal modulation frequency in LT is essential, a FFT analysis on the raw PuCT data was performed to qualitatively select the best frame and its corresponding frequency for each SUT. In particular, it has been found that the best frame is obtained at around 0.15 Hz for canvas and around 0.19 Hz for the panel. Therefore, LT was carried out using a sinusoid modulation at these frequencies using the same 110 W LED setup for 82 seconds, so as to be consistent with T_{SQ}, see Section IV. The results have been depicted in Fig.11 and Fig.12, which show the best frames obtained from FFT analysis (magnitude) on the acquired raw PuCT data and LT results respectively on both samples.

Embroideries are the most difficult defects to be detected due to their tiny dimension and the similarity to the surrounding canvas texture. Fig.13 shows the LT phase image of the canvas sample.

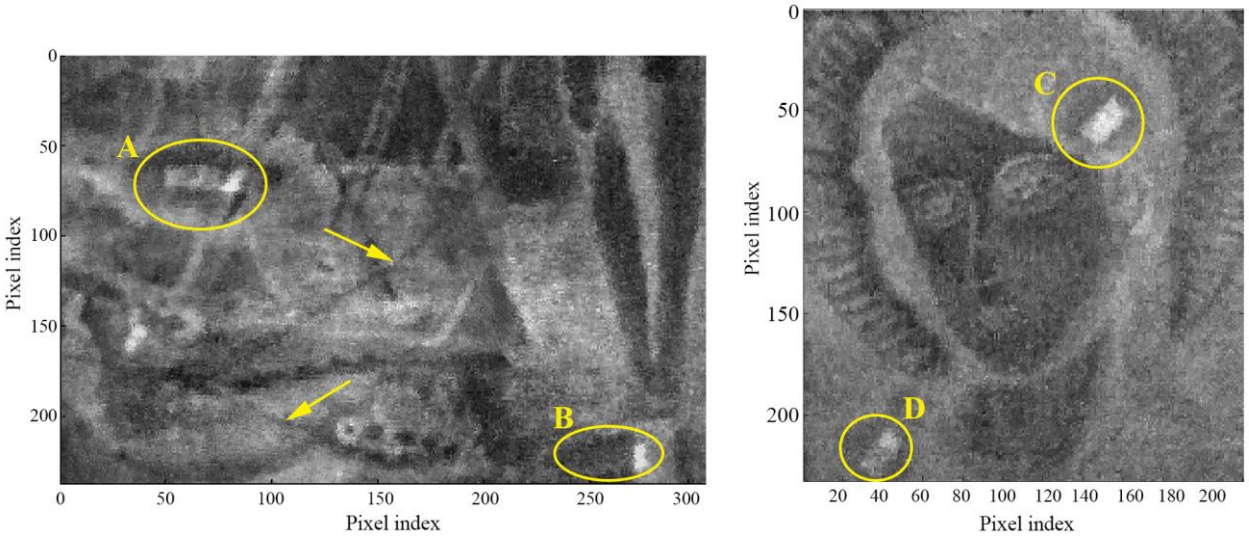

Fig. 11 Selected best frames after FFT (magnitude) for the (a) canvas at 0.15 Hz and (b) panel painting at 0.19 Hz.

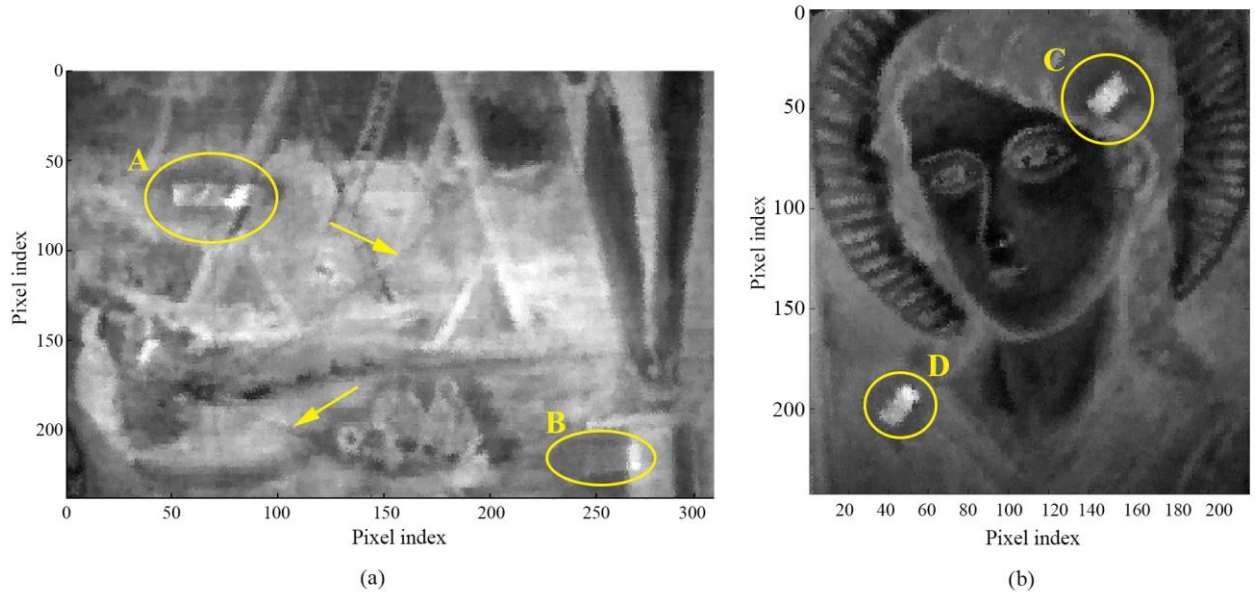

Fig. 12 Selected best frames (magnitude) after LT for the (a) canvas at 0.15 Hz and (b) panel painting at 0.19 Hz.

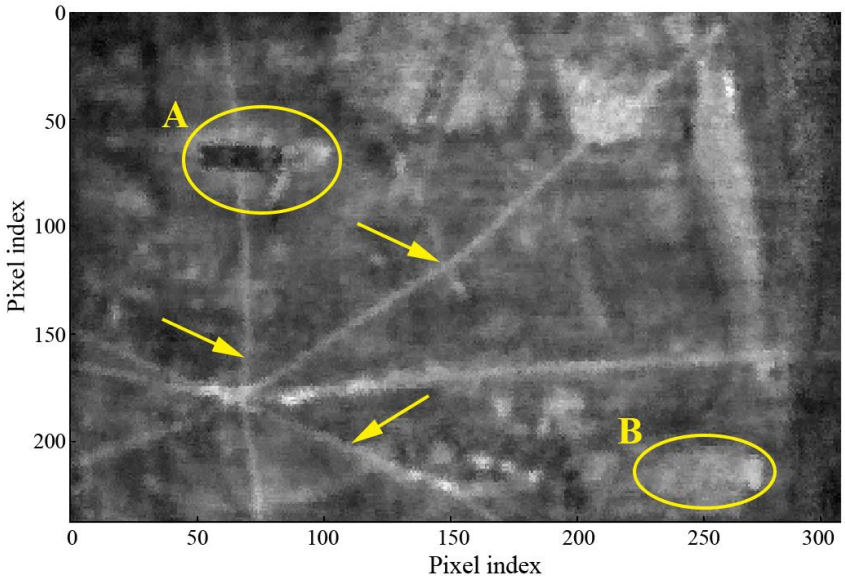

Fig. 13 Phase image after LT for the canvas painting.

VII. Discussion

The results obtained using the proposed PuCT approach are qualitatively comparable to the ones obtained by LT technique. This can be seen if Fig.10(a) and Fig.10(b) are compared with Fig.12(a) and Fig.12(b) respectively. In addition, it should be noted that the modulation frequency value used for LT should have been known a priori for the best result, whilst it has been chosen here after an FFT analysis of the PuCT raw data. The quality of the phase image obtained with LT on the canvas (Fig.13) is qualitatively comparable with the one obtained with PuCT on the same sample in time domain (Fig.10(a)). In fact, in both cases all the defects in the canvas are clearly visible.
Finally, the thermograms obtained from PuCT in Fig.8(b) and Fig.9(b) shows that a time analysis of the sample investigated features can be performed, as it is possible in PT.

VIII. Conclusions

In this work, the pulse compression technique was applied on paintings with the aim to detect subsurface defects. The technique was able to detect splitting areas located beneath various paint layers that were applied on panel and canvas supports. Recent strategies introduced in the scientific landscape able to improve the performance of the pulse-compression active thermography are explained; the experimental results linked to them demonstrate the gain provided by such procedures. The thermal impulse response of the inspected samples was reconstructed using an improved SNR and enhanced fidelity. A very low temperature difference causing a reasonable thermal stress on the upper layers was taken into account during thermographic inspections. Also, the type of penetration of the thermal waves appears sufficient to detect thin defects, such as crochet-work joins realized in the canvas. Future work intends to investigate coded excitations with an arbitrary power spectrum, further increasing the SNR of the deepest defects and reducing sidelobe levels.

Acknowledgments

The authors would like to thank Mr. Nino Zaccagnini (University of L'Aquila, Italy) who constructed the samples used in this work. Dr. Stefano Sfarra collaborated to the achievement of the canvas painting.

This research work has been partially supported from the European Union's Horizon 2020 research and innovation programme under the Marie Skłodowska-Curie grant agreement No 722134 - NDTonAIR"

REFERENCES

[1] Meola C, Carlomagno GM, Giorleo L. The use of infrared thermography for materials characterization. J Mater Process Technol 2004, 155:1132–1137.

[2] Weschenfelder A V., Maldague X, Rocha LM, Schaefer AL, Saucier L, Faucitano L. The use of infra-red thermography for pork quality prediction. Meat Sci 2014, 96:120-125.

[3] Sfarra S, Ibarra-Castanedo C, Paoletti D, Maldague X. Infrared vision inspection of cultural heritage objects from the city of l'Aquila, Italy and its surroundings. Mater Eval 2013,71.5.

[4] Ibarra-Castanedo C, Bendada A, Maldague X. Image and signal processing techniques in pulsed thermography. GESTS Int Trans Comput Sci Eng 2005, 22.1:89–100.

[5] Mercuri F, Cicero C, Orazi N, Paoloni S, Marinelli M, Zammit U. Infrared Thermography Applied to the Study of Cultural Heritage. Int J Thermophys 2015, 36.5-6:1189–1194.

[6] Mercuri F, Paoloni S, Orazi N, Cicero C, Zammit U. Pulsed infrared thermography applied to quantitative characterization of the structure and the casting faults of the Capitoline She Wolf. Appl Phys A Mater Sci Process 2017, 123.5:327.

[7] Gavrilov D, Maeva E, Grube O, Vodyanoy I, Maev R. Experimental comparative study of the applicability of infrared techniques for non-destructive evaluation of paintings. J Am Inst Conserv 2013, 52.1:48–60.

[8] Di Tuccio MC, Ludwig N, Gargano M, Bernardi A. Thermographic inspection of cracks in the mixed materials statue: Ratto delle Sabine. Herit Sci 2015, 3.1:10.

[9] Ibarra-Castanedo C, Sfarra S, Ambrosini D, Paoletti D, Bendada A, Maldague X. Diagnostics of panel paintings using holographic interferometry and pulsed thermography. Quant Infrared Thermogr J 2010, 7.1:85–114.

[10] Carlomagno GM, Meola C. Comparison between thermographic techniques for frescoes NDT. NDT&E Int 2002, 35.8: 559–565.

[11] Bendada A, Sfarra S, Ibarra-Castanedo C, Akhloufi M, Caumes JP, Pradere C, Batsale J, Maldague X. Subsurface imaging for panel paintings inspection: A comparative study of the ultraviolet, the visible, the Infrared and the terahertz spectra. Opto-Electronics Rev 2015, 23.1:90–101.

[12] Bodnar JL, Nicolas JL, Candoré JC, Detalle V. Non-destructive testing by infrared thermography under random excitation and ARMA analysis. Int. J. Thermophysics 2012, 33.10-11: 2011–2015.

[13] Mezghani S, Perrin E, Vrabie V, Bodnar JL, Marthe J, Cauwe B. Evaluation of paint coating thickness variations based on pulsed Infrared thermography laser technique. Infrared Phys Technol 2016, 76:393–401.

[14] Theodorakeas P, Avdelidis NP, Cheilakou E, Koui M. Quantitative analysis of plastered mosaics by means of active infrared thermography. Constr Build Mater 2014, 73:417–425.

[15] Sfarra S, Ibarra-Castanedo C, Theodorakeas P, Avdelidis NP, Perilli S, Zhang H, Nardi I, Koui M, Maldague X. Evaluation of the state of conservation of mosaics: Simulations and thermographic signal processing. Int J Therm Sci 2017, 117:287–315.

[16] Coccato A, Moens L, Vandenabeele P. On the stability of mediaeval inorganic pigments: A literature review of the effect of climate, material selection, biological activity, analysis and conservation treatments. Herit Sci 2017, 5.1:12.

[17] Frost RL, Weier ML, Martens W, Kloprogge JT, Ding Z. Dehydration of synthetic and natural vivianite. Thermochim Acta 2003, 401.2:121–130.

[18] Čermáková Z, Švarcová S, Hradilová J, Bezdička P, Lančok A, Vašutová V, Blažek J, Hradil D. Temperature-related degradation and colour changes of historic paintings containing vivianite. Spectrochim Acta - Part A Mol Biomol Spectrosc 2015, 140:101–110.

[19] Carlomagno GM, Berardi PG. Unsteady Thermotopography in Non-Destructive Testing. Proc 3rd Biannu Exch (IRIE '76) 1976, 24: 26.

[20] Kordatos EZ, Exarchos DA, Stavrakos C, Moropoulou A, Matikas TE. Infrared thermographic inspection of murals and characterization of degradation in historic monuments. Constr Build Mater 2013, 48:1261–1265.

[21] Maldague X. Theory and practice of infrared thermography for nondestructive testing. Wiley series in microwave and optical engineering. Wiley 2001.

[22] Maldague X, Marinetti S. Pulse phase infrared thermography. J Appl Phys 1996, 79.5:2694-2698.

[23] Beuve S, Qin Z, Roger JP, Holé S, Boué C. Open cracks depth sizing by multi-frequency laser stimulated lock-in thermography combined with image processing. Sensors Actuators A Phys 2016, 247:494–503.

[24] Tabatabaei N, Mandelis A. Thermal-wave radar: A novel subsurface imaging modality with extended depth-resolution dynamic range. Rev Sci Instrum 2009, 80.3:034902.

[25] Mulaveesala R, Tuli S. Theory of frequency modulated thermal wave imaging for nondestructive subsurface defect detection. Appl Phys Lett 2006, 89.19: 191913.
[26] Silipigni G, Burrascano P, Hutchins DA, Laureti S, Petrucci R, Senni L, Torre L, Ricci M. Optimization of the pulse compression technique applied to the infrared thermography nondestructive evaluation. NDT&E Int 2017, 87:100–110.
[27] Ricci M, Callegari S, Caporale S, Monticelli M, Battaglini L, Eroli M, Senni L, Rovatti R, Setti G, Burrascano P. Exploiting Non-Linear Chirp and sparse deconvolution to enhance the performance of pulse-compression ultrasonic NDT. IEEE Int Ultrason Symp IUS 2012, 1489–92.
[28] Hutchins D, Burrascano P, Davis L, Laureti S, Ricci M. Coded waveforms for optimised air-coupled ultrasonic nondestructive evaluation. Ultrasonics 2014, 54.7: 1745-1759.
[29] Mohamed I, Hutchins D, Davis L, Laureti S, Ricci M. Ultrasonic NDE of thick polyurethane flexible riser stiffener material. Nondestruct Test Eval 2017, 32.4:343–362.
[30] Laureti S, Ricci M, Mohamed MNIB, Senni L, Davis LAJ, Hutchins DA. Detection of rebars in concrete using advanced ultrasonic pulse compression techniques. Ultrasonics 2017, doi.org/10.1016/j.ultras.2017.12.010
[31] Mandelis A. Time-delay-domain and pseudorandom-noise photoacoustic and photothermal wave processes: a review of the state of the art. IEEE transactions on ultrasonics, ferroelectrics, and frequency control 1986, 33.5: 590-614.
[32] Candoré J. C, Bodnar J. L, Detalle V, Grossel P. Non-destructive testing of works of art by stimulated infrared thermography. The European Physical Journal Applied Physics 2012, 57.2: 21002.
[33] Yao Y, Sfarra S, Lagüela S, Ibarra-Castanedo C, Wu JY, Maldague XPV, Ambrosini D. Active thermography testing and data analysis for the state of conservation of panel paintings. Int J Therm Sci 2018, 126:143–151.
[34] Sfarra S, Theodorakeas P, Ibarra-Castanedo C, Avdelidis NP, Paoletti A, Paoletti D, Hrissagis K, Bendada A, Koui M, Maldague X. Evaluation of defects in panel paintings using infrared, optical and ultrasonic techniques. Insight Non-Destructive Test. Cond. Monit. 2012, 54.1: 21–27.
[35] Sfarra S, Ibarra-Castanedo C, Ambrosini D, Paoletti D, Bendada A, Maldague X. Discovering the defects in paintings using non-destructive testing (NDT) techniques and passing through measurements of deformation. J Nondestruct Eval 2014, 33.3:358–383.
[36] Zhang H, Sfarra S, Saluja K, Peeters J, Fleuret J, Duan Y, Fernandes H, Avdelidis N, Ibarra-Castanedo C, Maldague X. Non-destructive Investigation of Paintings on Canvas by Continuous Wave Terahertz Imaging and Flash Thermography. J Nondestruct Eval 2017, 36.2:34.
[37] Cennini C. The Craftsman's Handbook "Il Libro dell'Arte". Dover, 1933.
[38] Blake W. Acrylic Painting: A Complete Guide. Courier Corporation, 1997.
[39] Gettens RJ, Stout GL,. Painting materials : a short encyclopaedia. Dover Publications; 1966.
[40] Carslaw H, Jaeger J. Conduction of heat in solids. Oxford Clarendon Press 1959, 2nd edition 1959.
[41] Burgholzer P. Thermodynamic Limits of Spatial Resolution in Active Thermography. Int J Thermophys 2015, 36.9:2328–2341.
[42] Lopez F, De Paulo Nicolau V, Ibarra-Castanedo C, Maldague X. Thermal-numerical model and computational simulation of pulsed thermography inspection of carbon fiber-reinforced composites. Int J Therm Sci 2014, 86:325–340.
[43] Oelze ML. Bandwidth and resolution enhancement through pulse compression. IEEE Trans Ultrason Ferroelectr Freq Control 2007, 54.4.
[44] Sekko E, Thomas G, Boukrouche A. A deconvolution technique using optimal Wiener filtering and regularization. Signal Processing 1999, 72.1 :23–32.
[45] Haider B, Lewin PA, Thomenius KE. Pulse elongation and deconvolution filtering for medical ultrasonic imaging. IEEE Trans Ultrason Ferroelectr Freq Control 1998, 45.1:98–113.
[46] Gan TH, Pallav P, Hutchins D A. Non-contact ultrasonic quality measurements of food products. J Food Eng 2006, 77.2:239–247.
[47] Arora V, Mulaveesala R. Pulse compression with gaussian weighted chirp modulated excitation for infrared thermal wave imaging. Prog Electromagn Res Lett 2014, 44:133–137.
[48] Burrascano P, Laureti S, Ricci M, Senni L, Silipigni G, Tomasello R. Reactance transformation to improve range resolution in pulse-compression detection systems. 2017 40th Int. Conf. Telecommun. Signal Process., IEEE; 2017, p. 480–483.
[49] Pallav P, Gan TH, Hutchins DA. Elliptical-Tukey Chirp Signal for Ultrasonic Imaging. IEEE Trans Ultrason Ferroelectr Freq Control 2007, 54.8.
[50] Burrascano P, Callegari S, Montisci A, Ricci M, Versaci M. Ultrasonic Nondestructive Evaluation Systems: Industrial Application Issues. Springer, 2014.
[51] Burrascano P, Laureti S, Senni L, Ricci M. Range Sidelobes Reduction for Pulse-Compression NDT based on Reactance Transformation, IEEE International Symposium of Circuits & Systems 2018, Florence 27-30 May 2018, Italy (accepted)